LETTERS

Effect of remote sea surface temperature change on tropical cyclone potential intensity

Gabriel A. Vecchi[1] & Brian J. Soden[2]

The response of tropical cyclone activity to global warming is widely debated[1–10]. It is often assumed that warmer sea surface temperatures provide a more favourable environment for the development and intensification of tropical cyclones, but cyclone genesis and intensity are also affected by the vertical thermodynamic properties of the atmosphere[1,10–13]. Here we use climate models and observational reconstructions to explore the relationship between changes in sea surface temperature and tropical cyclone 'potential intensity'—a measure that provides an upper bound on cyclone intensity[10–14] and can also reflect the likelihood of cyclone development[15,16]. We find that changes in local sea surface temperature are inadequate for characterizing even the sign of changes in potential intensity, but that long-term changes in potential intensity are closely related to the regional structure of warming; regions that warm more than the tropical average are characterized by increased potential intensity, and vice versa. We use this relationship to reconstruct changes in potential intensity over the twentieth century from observational reconstructions of sea surface temperature. We find that, even though tropical Atlantic sea surface temperatures are currently at a historical high, Atlantic potential intensity probably peaked in the 1930s and 1950s, and recent values are near the historical average. Our results indicate that—per unit local sea surface temperature change—the response of tropical cyclone activity to natural climate variations, which tend to involve localized changes in sea surface temperature, may be larger than the response to the more uniform patterns of greenhouse-gas-induced warming.

Potential intensity (PI) represents a theoretical upper limit on the intensity of tropical cyclones based on sea surface temperature (SST) and the local vertical thermodynamic structure of the atmosphere[10–12]. With all other factors being equal, a local warming of SST would act to destabilize the overlying atmosphere and increase PI (refs 1,10–13). However, remote SST changes can also influence PI through their influence on upper atmospheric temperatures[1,17]. In the tropical free troposphere, where the Coriolis force is weak, temperature gradients are small and, on timescales longer than a few months, upper tropospheric temperature anomalies are determined by changes in the tropical-mean SST[18]. Thus, local PI in the tropics is influenced by both local and remote SST changes[1,17]. This can be seen on interannual timescales, with Pacific warming leading to increased stability in the tropical Atlantic and contributing to reduced tropical cyclone activity[19], even though Atlantic SSTs are anomalously warm during El Niño.

The effects of local and remote surface warming on PI changes are clearly evident in climate model projections of the twenty-first century performed for the Fourth Assessment Report of the Intergovernmental Panel on Climate Change (IPCC-AR4; see Fig. 1). Tropical SST is projected to warm everywhere in response to the increasing greenhouse gases, although the warming is not spatially homogeneous (Fig. 1a). The maximum warming is along the Equator, the Northern Hemisphere warms more than the Southern, and the largest area of warming is in the Indo-Pacific. In the Northern Hemisphere Atlantic, a local minimum in warming covers a broad area, extending from the Caribbean Sea to the northwest coast of Africa. In contrast to the SST, which increases everywhere, the changes in PI are mixed, with regions of both increase and decrease (Fig. 1b). PI is projected to increase in most regions of tropical cyclone activity during the months considered (June–November), except over a broad region in the tropical North Atlantic, where it decreases despite substantial warming. The projections of northern tropical Atlantic PI change show regions of both large increase and moderate decrease. This figure emphasizes that warmer SSTs, by themselves, do not necessarily indicate a more favourable thermodynamic environment for tropical cyclone intensity[1]. This behaviour is highlighted by the contours in Fig. 1b, which show the departure of local SST change from the tropical mean. Notice that decreased PI is associated with regions that warm less than the tropical mean and vice versa. The differing behaviour of PI and SST is also evident in time series of the PI response to global warming (Fig. 2 illustrates the behaviour with one model; Supplementary Figs 1–3 show the 22 IPCC-AR4 models used). Local SSTs increase steadily in the tropics, whereas PI shows large decadal variability, and may increase, decrease or show no change in the long term.

Potential intensity can be computed from atmospheric observational analysis products[20,21] since 1958. The regional structure of PI trends in reanalysis products, and the difference between the two products, can be attributed largely to the regional structure of the SST changes (Supplementary Fig. 4). Because the stabilizing effects of remote SST changes can be estimated by the tropical-mean SST change, regions that warm more (less) than the tropical mean show an increase (decrease) of PI, a behaviour similar to that in model projections of global warming (Fig. 1b).

These results suggest that, when vertical atmospheric profiles are unavailable, the departure of local SST changes from tropical-mean SST changes can be used as a surrogate for PI. Although PI is straightforward to compute, it is dependent on the availability of vertical temperature and humidity data. This is not an issue for model simulations, but it can become problematic for historical reconstructions because observations of vertical profiles of temperature and humidity are only available since the mid-twentieth century and are subject to discontinuities in sampling and data quality. Thus problems may exist with multi-decadal trends computed from data that span large changes in observational practices[12].

Here we make use of the relationship between PI and the local departure from tropical SST change to develop a proxy index for

[1]Geophysical Fluid Dynamics Laboratory, NOAA, Princeton, New Jersey 08542, USA. [2]Rosenstiel School for Marine and Atmospheric Science, University of Miami, Miami, Florida 33149, USA.

changes in PI ($\tilde{P}I$, see Methods and Supplementary Information). Observational SST reconstructions[22–24] from the 1870s onwards are used to assess the implications of historical SST for long-term changes in PI. Because regional aspects of the long-term changes in SST differ across the reconstructions[25], we explore the $\tilde{P}I$ changes shown by three different reconstructions (ERSST[22], HadISST[23] and Kaplan[24]; see Supplementary Information) to assess how differences between reconstructions affect $\tilde{P}I$. In Fig. 3 we show the spatial structure of changes for ref. 22, and those of the other two products in Supplementary Fig. 5.

Between the late nineteenth century and the early twenty-first century, June–November SST has increased throughout the tropics (Fig. 3a, Supplementary Fig. 5). The largest warming has been in the northern and near-equatorial Indian Ocean, and the southern tropical and near-equatorial Atlantic.

In contrast to the SST trends, which are overwhelmingly positive, trends in June–November $\tilde{P}I$ (Fig. 3b and Supplementary Fig. 5) are mixed, highlighting the spatial heterogeneity of the warming and suggesting that the long-term changes in PI have included regions of both increase and decrease. For example, all products show an increase in $\tilde{P}I$ in the northern Indian Ocean, a decrease in the western tropical Pacific, and mixed changes in the tropical Atlantic (with regions of both increase and decrease). Thus, even in the presence of warming ocean temperatures over the last century, $\tilde{P}I$ suggests that the thermodynamic environment in many regions has become less favourable for intensification of tropical cyclones.

Figure 4 shows time series of SST and $\tilde{P}I$ for the three regions used in Supplementary Fig. 1 and highlighted in Fig. 1a. All three SST data sets indicate substantial warming in the three regions over the twentieth century. In the Atlantic sector, SSTs have been at unprecedented levels since the late 1990s, yet the tropical Atlantic $\tilde{P}I$ is at near-average levels for that period, and had its highest levels during the middle of the twentieth century (Fig. 4c). The only long-term increase in $\tilde{P}I$ has been in the Indian Ocean, and recent Pacific $\tilde{P}I$ has been lower than the long-term mean (the decrease arising abruptly in the 1970s).

The combined influence of local and remote SST changes on $\tilde{P}I$ can be seen clearly in the Atlantic basin. Atlantic $\tilde{P}I$ began to decrease in the mid-1950s, even though local SST was not changing substantially ($\tilde{P}I$ decreases by 0.6–0.7 °C from the 1950s to the 1980s, while local SST decreases by only 0.1–0.2 °C). This reduction in $\tilde{P}I$ was not dominated by a local SST decrease, but by the rapid warming elsewhere in the tropics (much of it in the Indian Ocean). Until recently, the warming of the Indian Ocean has acted to stabilize the atmosphere elsewhere in the tropics, modulating the $\tilde{P}I$ changes that would have otherwise occurred. In the most recent decades (over which Atlantic hurricane intensities have increased[2,4,5,7]) $\tilde{P}I$ has increased substantially in the Atlantic, as the warming of the

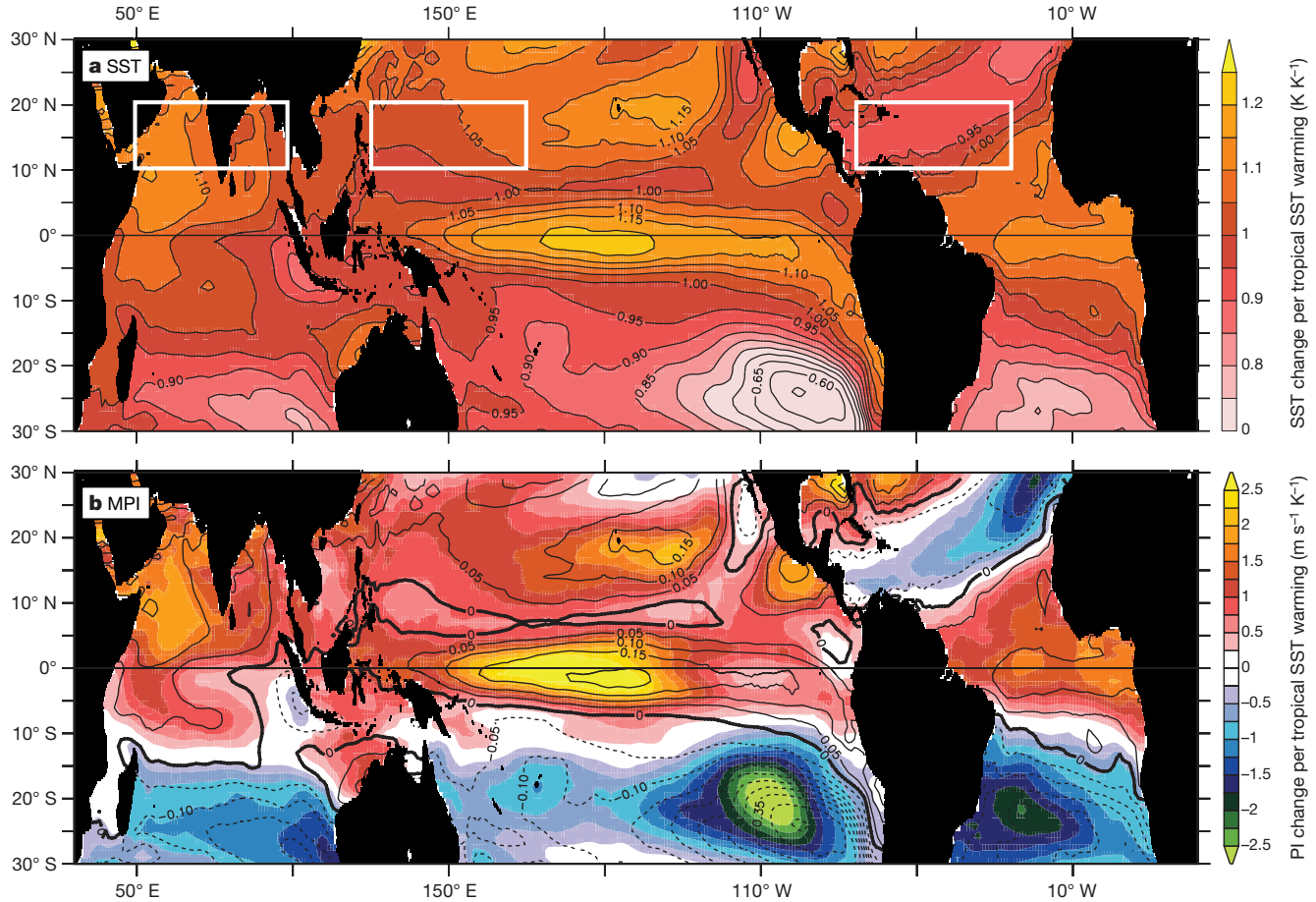

Figure 1 | Spatial structure of model-projected changes in SST and PI for the twenty-first century. The panels show multi-model projections from the IPCC-AR4 emissions scenario A1B (see Methods; this model archive is now known as the World Climate Research Programme Coupled Model Inter-comparison Project 3 database, or CMIP-3). Projections of June–November change per °C tropical warming in **a**, SST (°C °C^{-1}), and **b**, PI (shaded, in m s^{-1} °C^{-1}; ref. 11) and in the normalized departure of the local SST change from the tropical-mean SST change (contoured, in °C °C^{-1}). MPI, maximum PI. The spatial correlation coefficient between SST and PI changes is $r = 0.84$. Changes are normalized by each model's global mean June–November surface air temperature change before averaging. Boxes indicate three regions with time series shown in Fig. 4. This general pattern of surface warming is a robust result of the IPCC-AR4 model projections for the twenty-first century: all of the models show a maximum warming along the Equator[26] and the meridional asymmetry across the Equator, and 16 of those 22 models show the local minimum in the North Atlantic.

Indian Ocean has lessened but warming in the Atlantic has accelerated. Even though Atlantic PI changes since the 1950s have not tracked those of SST, Atlantic tropical cyclone activity has shown a pronounced increase and tracked SST since the 1950s (refs 2,4,10), suggesting that the tropical cyclone activity changes involve factors other than PI as derived in ref. 11, such as vertical wind shear or atmospheric humidity[2,6,9,10,25].

The rapid twentieth -century warming of the Indian Ocean had a different effect on $\tilde{PI}$ locally than it did on the Atlantic. As Indian Ocean SSTs warmed rapidly between the mid-1950s and the 1990s they were tracked by an increase in local $\tilde{PI}$. In recent years, Indian Ocean temperatures have remained relatively steady while the rest of the tropics have continued to warm, and this has led to a decrease in Indian Ocean $\tilde{PI}$.

Although $\tilde{PI}$ is able to capture much of the structure of PI changes, it cannot describe tropical-mean changes in PI. However, regional changes in PI tend to be substantially larger in magnitude than tropical-mean changes, and tropical-mean PI changes can be positive or negative and are poorly constrained by tropical-mean SST changes (see Supplementary Fig. 6). The response of tropical-mean MPI is nominally positive for the models shown in Fig. 1, but is not significantly different from zero given the large inter-model spread; efforts should be undertaken to understand and constrain changes in tropical-mean PI.

These results emphasize the importance of understanding the regional structure of SST changes in response to anthropogenic forcing. For example, the projected increase in Northern Hemisphere June–November PI in response to increased CO_2 (Fig. 1b) is not tied to the 'global' nature of the warming (see Supplementary Fig. 6), but rather to the fact that the model warming shows a meridional asymmetry, being larger in the Northern Hemisphere tropics (Fig. 1a). The prominent decreases in PI in the subsiding regions of the Southern Hemisphere (Fig. 1b) would not directly influence storm intensity (as tropical cyclones do not typically form in those regions), yet the remote influence of the Southern Hemisphere minimum in warming would be to enhance the PI increase in the Northern Hemisphere. The equatorial intensification of tropical ocean warming in model projections for the twenty-first century[26] places the maximum tropical PI increase equatorward of 5° latitude, where planetary vorticity is of small amplitude and thus limits the direct impact of the largest projected SST increases on tropical cyclones; however, the large projected near-equatorial warming also acts to moderate remote PI increases.

A corollary of these results is that localized SST changes are more effective at altering PI than a more uniform temperature change of the same magnitude (see Supplementary Information). This suggests that surface temperature changes driven by well-mixed greenhouse gases, for which local changes in the tropics are dominated by a mean warming (Fig. 1a), will be less effective at modifying PI (per degree local warming) than those driven by internal modes of climate variability, which tend to have much larger spatial gradients in surface warming. For example, given the regional nature of the SST changes associated with the Atlantic Multi-decadal Oscillation[6], the Atlantic Meridional Mode[27], variations of the Atlantic Warm Pool[28] or

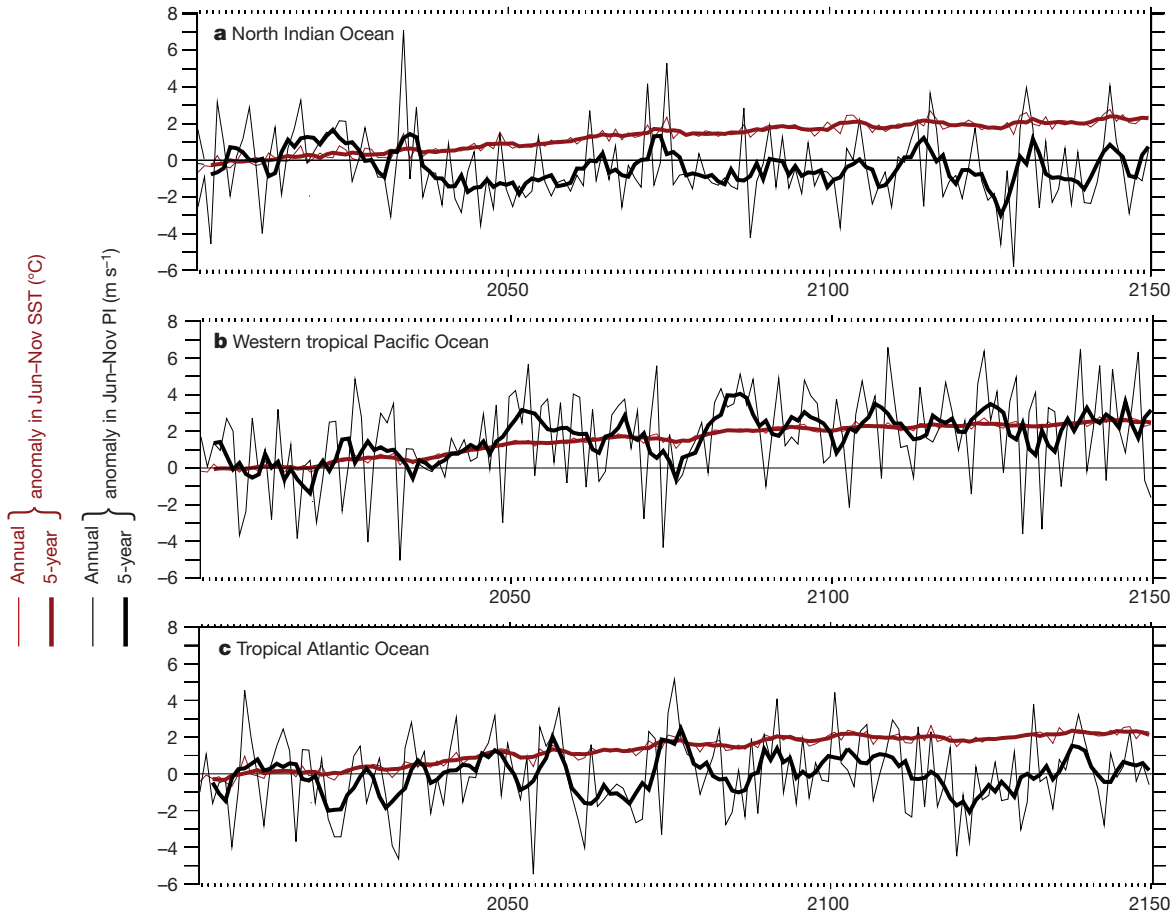

Figure 2 | Time series of June–November change in SST and PI. Changes in SST (red lines, °C) and PI as derived in ref. 11 (black lines, m s^{-1}) are from the GFDL CM2.1 scenario A1B projection in Northern Hemisphere tropical regions (see Fig. 1a). Thin lines show the annual values, thick lines show the 5-yr running mean. Changes calculated from 2001–2020 average. Time series of the changes in SST and PI over these regions for all 22 IPCC-AR4 models can be seen in Supplementary Figs 1–3. Notice that although SST warms steadily in each tropical region, PI shows substantial variability on many timescales, which can overwhelm the long-term change.

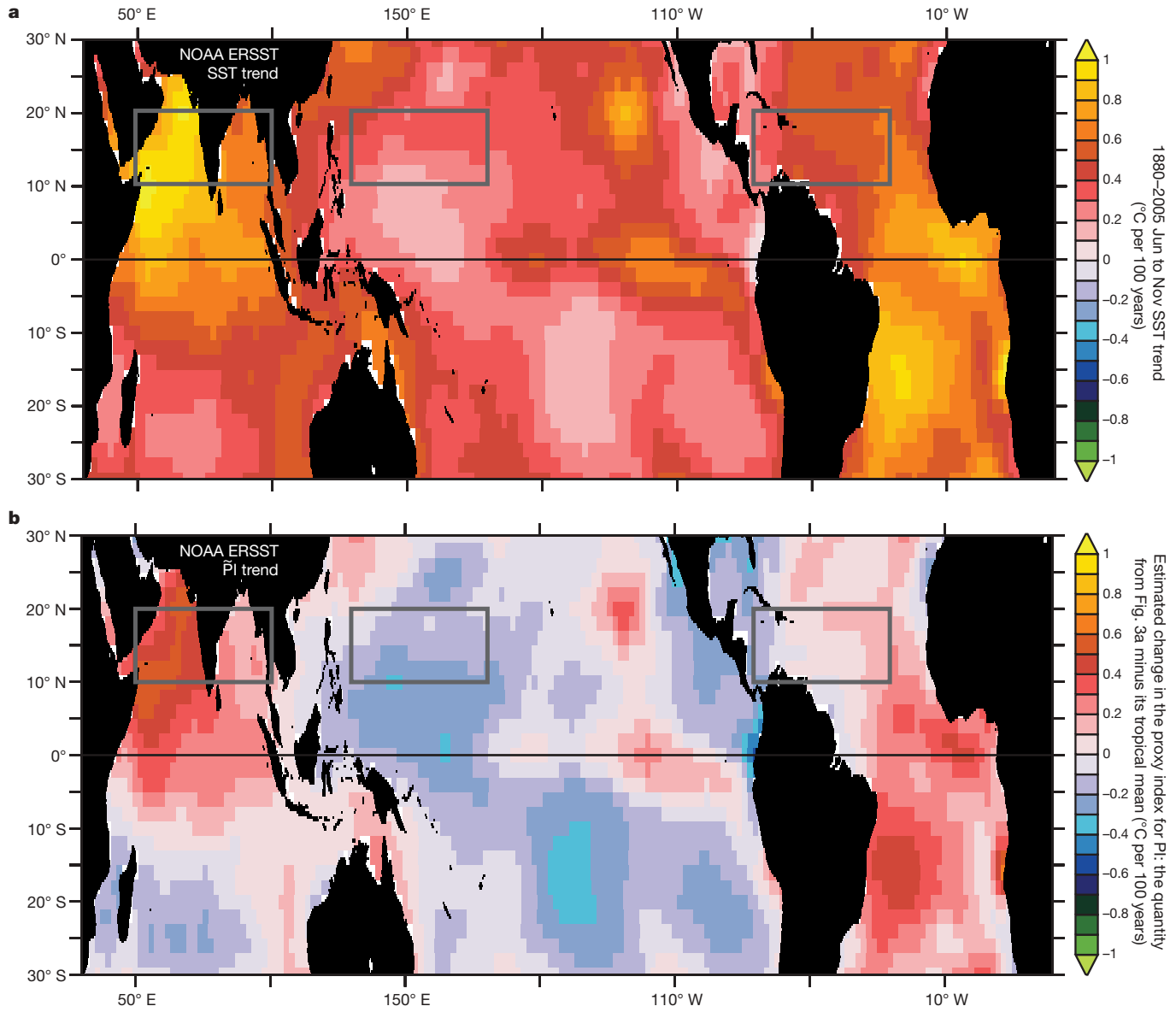

Figure 3 | Century-scale trends in SST and an estimate for PI. **a**, Linear trend from 1880 to 2006 in June–November SST and **b**, departure of local SST from tropical-mean SST, calculated using the SST reconstructions of ref. 22. See Supplementary Fig. 5 for equivalent figures using refs 24 and 25. Units are °C per century.

differential temperature changes in the Indo-Pacific and Atlantic basins[8], these climate variations should have considerable impact on Atlantic PI in addition to their associated wind shear changes—much as El Niño does[19]. Thus, because of their combined influence of wind shear and PI, these modes of climate variability should have a substantial impact on tropical cyclone activity. More speculatively, given the inhomogeneous character of model[29] and observational[30] estimates of SST anomalies during the Last Glacial Maximum, one may expect that there may have been regions where PI was larger than today, even though the world was considerably colder.

METHODS SUMMARY

We use the potential intensity (PI) derived in ref. 11 to characterize the large-scale thermodynamic environment for tropical cyclone intensification. From model and reanalysis data we compute PI using monthly mean atmospheric temperature, specific humidity, sea level pressure and sea surface temperature (SST) data, and the algorithm available at http://wind.mit.edu/~emanuel/home.html.

We explore changes of SST and PI projected for the twenty-first century using a suite of coupled ocean–atmosphere models forced by emissions scenario A1B (a mid-range emissions scenario, with atmospheric CO_2 stabilization at 720 p.p.m. by year 2100) for the IPCC-AR4. We compute differences between two 20-yr periods: 2001–2020 and 2081–2100. We produce a multi-model ensemble by averaging the response of 22 coupled general circulation models. See online Methods Section for more details. These models do not explicitly resolve the details of tropical cyclones.

Across the reanalyses and the IPCC-AR4 model projections, long-term changes in the difference between local and tropical-mean SST change are strongly correlated with those in local PI ($r \approx 0.8$), and the linear regression fit between the two has a near-zero intercept (see Supplementary table). So we define a proxy index for PI ($\tilde{P}I$) as the difference between local and tropical-mean SST change. Further, the slope of the linear regression fit of PI to $\tilde{P}I$ in June–November is similar in the IPCC-AR4 multi-model ensemble (8.2 m s^{-1} per °C, although it can vary between models; see Supplementary Information) and the reanalyses (8.6 and 8.2 m s^{-1} per °C for refs 21 and 22, respectively), so we use a slope of 8 m s^{-1} to estimate the wind speed equivalent.

By construction, the tropical-mean trend in $\tilde{P}I$ must be 0, whereas tropical-mean PI changes can be slightly non-zero. However, both model projections and historical reanalyses indicate that the tropical-mean multi-decadal changes in PI are typically substantially smaller than the prominent regional changes (see Supplementary Information).

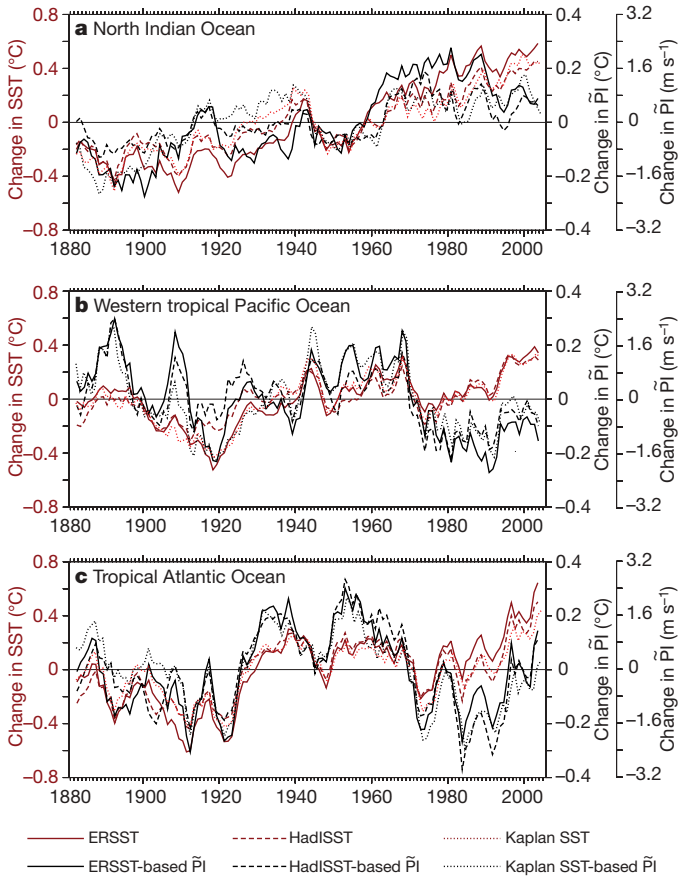

Figure 4 | Anomalies in SST and estimated PI since the late nineteenth century. Regional averages of 5-yr running averaged anomalies in June–November SST (red) and $\tilde{P}I$ (black) based on reconstructions of SST in ref. 23 (solid lines), ref. 24 (dashed lines) and ref. 25 (dotted lines). Units for SST are °C, and those for $\tilde{P}I$ are either °C or m s^{-1} when the regression coefficient between $\tilde{P}I$ and PI from the reanalyses and climate model ensemble-mean is used (~8 m s^{-1} per °C; see Supplementary Information). Anomalies are calculated from the 1880–2006 average.

Full Methods and any associated references are available in the online version of the paper at www.nature.com/nature.

Received 23 July; accepted 26 October 2007.

1. Shen, W., Tuleya, R. E. & Ginis, I. A sensitivity study of the thermodynamic environment on GFDL model hurricane intensity: Implications for global warming. *J. Clim.* **13,** 109–121 (2000).
2. Goldenberg, S. B., Landsea, C., Mestas-Nunez, A. M. & Gray, W. M. The recent increase in Atlantic hurricane activity. *Science* **293,** 474–479 (2001).
3. Knutson, T. R. & Tuleya, R. E. Impact of CO_2-induced warming on simulated hurricane intensity and precipitation: Sensitivity to the choice of climate model and convective parameterization. *J. Clim.* **17,** 3477–3495 (2004).
4. Emanuel, K. A. Increasing destructiveness of tropical cyclones over the past 30 years. *Nature* **436,** 686–688 (2005).
5. Webster, P. J., Holland, G. J., Curry, J. A. & Chang, H.-R. Changes in tropical cyclone number, duration and intensity in a warming environment. *Science* **309,** 1844–1846 (2005).
6. Zhang, R. & Delworth, T. L. Impact of Atlantic multidecadal oscillations on India/Sahel rainfall and Atlantic hurricanes. *Geophys. Res. Lett.* **33,** L17712, doi:10.1029/2006GL026267 (2006).
7. Knutson, T. R., Sirutis, J. J., Garner, S. T., Held, I. M. & Tuleya, R. E. Simulation of the recent multi-decadal increase of Atlantic hurricane activity using an 18-km grid regional model. *Bull. Am. Meteorol. Soc.* **88** (10), 1549–1565 (2007).
8. Latif, M., Keenlyside, N. & Bader, J. Tropical sea surface temperature, vertical wind shear, and hurricane development. *Geophys. Res. Lett.* **34,** L01710, doi:10.1029/2006GL027969 (2007).
9. Vecchi, G. A. & Soden, B. J. Increased tropical atlantic wind shear in model projections of global warming. *Geophys. Res. Lett.* **34,** L08702, doi:10.1029/2006GL028905 (2007).
10. Emanuel, K. A. Environmental factors affecting tropical cyclone power dissipation. *J. Clim.* (in the press).
11. Bister, M. & Emanuel, K. A. Dissipative heating and hurricane intensity. *Meteorol. Atmos. Phys.* **65,** 233–240, doi:10.1007/BF01030791 (1998).
12. Bister, M. & Emanuel, K. A. Low frequency variability of tropical cyclone potential intensity. 1. Interannual to interdecadal variability. *J. Geophys. Res.* **107,** 4801, doi:10.1029/2001JD000776 (2002).
13. Holland, G. J. The maximum potential intensity of tropical cyclones. *J. Atmos. Sci.* **54,** 2519–2541 (1997).
14. Emanuel, K. A statistical analysis of tropical cyclone intensity. *Mon. Weath. Rev.* **128,** 1139–1152 (2000).
15. Emanuel, K. A. & Nolan, D. S. Tropical cyclones and the global climate system. In *26th Conf. Hurricanes and Tropical Meteorology (American Meteorological Society, Miami, 2004)*. ⟨ftp://texmex.mit.edu/pub/emanuel/PAPERS/em_nolan_extended_2004.pdf⟩
16. Camargo, S. J., Emanuel, K. A. & Sobel, A. H. Use of genesis potential index to diagnose ENSO effects upon tropical cyclone genesis. *J. Clim.* **20,** 4819–4834 (2007).
17. Elsner, J. B., Tsonis, A. A. & Jagger, T. H. High-frequency variability in hurricane power dissipation and its relationship to global temperature. *Bull. Am. Meteorol. Soc.* **87,** 763–768 (2006).
18. Sobel, A. H., Held, I. M. & Bretherton, C. S. The ENSO signal in tropical tropospheric temperature. *J. Clim.* **15,** 2702–2706 (2002).
19. Tang, B. H. & Neelin, J. D. ENSO Influence on Atlantic hurricanes via tropospheric warming. *Geophys. Res. Lett.* **31,** L24204, doi:10.1029/2004GL021072 (2004).
20. Uppala, S. M. *et al.* The ERA-40 reanalysis. *Q. J. R. Meteorol. Soc.* **131,** 2961–3012 (2005).
21. Kalnay, E. *et al.* The NMC/NCAR 40-year reanalysis project. *Bull. Am. Meteorol. Soc.* **77,** 437–471 (1996).
22. Smith, T. M. & Reynolds, R. W. Extended reconstruction of global sea surface temperatures based on COADS data (1854–1997). *J. Clim.* **16,** 1495–1510 (2003).
23. Rayner, N. A. *et al.* Global analyses of sea surface temperature, sea ice, and night marine air temperature since the late nineteenth century. *J. Geophys. Res.* **108,** doi:10.1029/2002JD002670 (2003).
24. Kaplan, A. *et al.* Analyses of global sea surface temperature 1856–1991. *J. Geophys. Res.* **103,** 18567–18589 (1998).
25. Vecchi, G. A. & Soden, B. J. Global warming and the weakening of the tropical circulation. *J. Clim.* **20,** 4316–4340 (2007).
26. Liu, Z., Vavrus, S., He, F., Wen, N. & Zhong, Y. Rethinking tropical ocean response to global warming: The enhanced equatorial warming. *J. Clim.* **18,** 4684–4700 (2005).
27. Vimont, D. J. & Kossin, J. P. The Atlantic Meridional Mode and hurricane activity. *Geophys. Res. Lett.* **34,** L07709, doi:10.1029/2007GL029683 (2007).
28. Wang, C., Enfield, D. B., Lee, S.-K. & Landsea, C. W. Influences of the Atlantic warm pool on western hemisphere summer rainfall and Atlantic hurricanes. *J. Clim.* **19,** 3011–3028 (2006).
29. Broccoli, A. Tropical cooling at the Last Glacial Maximum: An atmosphere–mixed layer ocean model simulation. *J. Clim.* **13,** 951–976 (2000).
30. CLIMAP Project Members. The last interglacial ocean. *Quat. Res.* **21,** 123–224 (1984).
31. Gualdi, S., Scoccimarro, E., Bellucci, A., Grezio, A., Manzini, E. & Navarra, A. The main features of the 20th century climate as simulated with the SGX coupled GCM. *Claris News* **4,** 7–13 (2006).
32. Gordon, H. B. *et al. The CSIRO Mk3 Climate System Model*. Tech. Report 60 (CSIRO Atmospheric Research, Aspendale, Victoria, 2002).

Supplementary Information is linked to the online version of the paper at www.nature.com/nature.

Acknowledgements We acknowledge the various modelling groups for providing their data, and PCMDI and the IPCC Data Archive at LLNL/DOE for collecting, archiving and making the data readily available. We thank T. Delworth, K. Dixon, S. Garner, D. E. Harrison, I. Held, A. E. Johansson, T. Knutson, R. Stouffer, A. Wittenberg, S. Ilcane and A. Laperra for discussion, and K. Emanuel for comments. This work was partially supported by NASA and NOAA-OGP.

Author Information Reprints and permissions information is available at www.nature.com/reprints. Correspondence and requests for materials should be addressed to G.A.V. (Gabriel.A.Vecchi@noaa.gov).

METHODS

We use the thermodynamic potential intensity for tropical cyclones derived by refs 11 and 12 to characterize the large-scale thermodynamic environment for tropical cyclone intensification. From model and reanalysis data we compute PI using monthly-mean atmospheric temperature, specific humidity, sea level pressure and sear surface temperature (SST) data, and the algorithm available at http://wind.mit.edu/~emanuel/home.html.

To explore twenty-first-century projected changes of SST and PI, we use a suite of coupled ocean–atmosphere models forced by emissions scenario A1B (a mid-range emissions scenario, with atmospheric CO_2 stabilization at 720 p.p.m. by year 2100) for IPCC-AR4. We calculate between two 20-yr periods: 2001–2020 and 2081–2100. We produce a multi-model ensemble by averaging the response of 22 coupled general circulation models (the 20 models with three-dimensional atmospheric data used by ref. 9 and described in Table 1 of ref. 26, along with the INGV (ref. 31) and CSIRO-Mk3.5 (ref. 32) models that became available more recently in the IPCC-AR4 database). We also look at two additional emissions scenarios (A2 and B1, with atmospheric CO_2 levels at 2100 of 855 p.p.m. and 550 p.p.m., respectively) to explore the relationship between tropical-mean changes in PI and SST. These models are generally of relatively coarse resolution and do not explicitly resolve tropical cyclone dynamics, but they are able to represent aspects of large-scale climate conditions that are relevant to tropical cyclone genesis and intensification, such as the thermodynamic structure of the atmosphere.

To examine observed changes in PI and SST relative to the late 1950s we use data from the European Centre for Medium Range Weather Forecasting 40-year Atmospheric Reanalysis (ERA40; ref. 20) and from the US National Center for Environmental Prediction (NCEP) Atmospheric Reanalysis (ref. 21). For each reanalysis product long-term changes are computed as linear least-squares trends over the period 1958–2002. As these two model-based atmospheric observational reanalyses are affected by data discontinuities and a changing observing system, it has been argued that these changes affect the validity of the PI values that are calculated from these analyses[12]. Nevertheless, we explore the relationship between changes in SST and PI in these products, to find an 'observational' analogue for the projections of future climate change of the IPCC-AR4 models. It is possible that the overall tendency for a tropical-mean decrease in PI in these products is due to inhomogeneity in observing practices[12], yet the tropical-mean changes in PI are small relative to the regional changes—which are the focus of this study (see Section IV of the Supplementary Information).

We calculate long-term changes in historical SST over the period 1880–2005, using statistical reconstructions of instrumental data, which take historical observed SST data and use statistical methods to reconstruct global gridded data sets. Because the long-term trends in different SST reconstructions can differ[25], we use three historical reconstruction products: the US National Oceanic and Atmospheric Administration Extended Reconstruction of SST (NOAA-ERSST; ref. 22); the UK Meteorological Office Hadley Centre Interpolated SST product (HadISST; ref. 23); and the Columbia University Lamont-Doherty Earth Observatory's Historical SST Recontruction (Kaplan SST; ref. 24).

These three SST products differ in their analysis procedure, with different statistical reconstruction methods used to estimate the value of SST in regions with no data. Also, the methods differ in the corrections applied to the data to account for changes in observing practices (such as going from 'bucket temperature measurements', where the temperature of water taken using buckets was measured, to 'ship intake' temperatures, where the temperature of the water in the engine room intake was measured, to 'hull sensor' measurements, where measurements of temperature are made using sensors mounted on the hulls of ships), with HadISST and Kaplan sharing a correction algorithm that differs from that of ERSST. These data sets also use slightly different data sources (for example, the NOAA product uses only *in situ* measurements over the whole record, whereas the source data for Kaplan and HadISST include satellite-derived SST starting in the early 1980s; the source data for Kaplan and HadISST include additional *in situ* observations from the Met Office archive not present in the NOAA product). Although the overall tendency for SST warming is robust, there are discrepancies in the spatial structure of the changes in all three tropical basins. Until the disagreement between the various SST records is resolved, we believe it prudent to examine all three and view their differences as an estimate of the uncertainty in SST. The true uncertainty in SST is larger than the discrepancy between these SST products, as they share many common elements, so their differences are a lower-bound estimate in uncertainty. Also, and almost self-evidently, the further one extends the record back in time, the larger the uncertainty. Nonetheless, these observationally based estimates of SST allow us to estimate the changes in conditions in the tropics since the late nineteenth century.

Supplementary Material to: Effect of remote sea surface temperature change on tropical cyclone potential intensity

Gabriel A. Vecchi

Geophysical Fluid Dynamics Laboratory –NOAA

Brian J. Soden

Rosenstiel School for Marine and Atmospheric Science – U. Miami

Nature (2007)

Corresponding author: Dr. Gabriel A. Vecchi, Geophysical Fluid Dynamics Laboratory / NOAA, US Route 1, Forrestal Campus, Princeton, NJ 08542
Tel: (609) 452-6583, Fax: (609) 987-5063, email: gabriel.a.vecchi@noaa.gov

I. Time-series of PI and SST from a climate model projection:

Figure 1 of the main text highlighted the difference in the multi-model ensemble projections of June-November sea surface temperature (SST) and tropical cyclone potential intensity (PI, *Bister and Emanuel [1998, 2002]*), in that the tropics warms everywhere, but there are regions where PI decreases. In Figure 2 of the main text we further highlighted the differing behavior of PI and SST through time-series of June-November SST and PI for 150 years of the Scenario A1B run using the GFDL CM2.1, using time-series of PI and SST averaged over three regions in the northern hemisphere tropics: the north Indian Ocean (10°N-20°N, 50°E-100°E), the western tropical Pacific (10°N-20°N, 130°E-180°) and the tropical Atlantic (10°N-20°N, 80°W-30°W); these regions are highlighted with boxes in Figure 1.a. In each of the regions the SST increases steadily relative the internal variability, but PI changes do not follow the monotonic

increase of SST. In each of the basins the decadal and interannual variability of PI is larger, relative to the long-term changes, than that of SST.

For GFDL CM2.1, only in the west Pacific does the character of the PI time-series resemble that of the SST. For the PI computed from this particular model the Atlantic and Indian Oceans the decadal variability is larger than the secular trend, but in the Pacific Ocean the decadal variability is smaller than the long-term increase in PI but still substantial. Additionally, the interannual variability is larger than the long-term changes in each of the three regions: though June-November SST does not return to its 2001-2020 average after 2030 in any of the regions, the year-to-year PI variations cross the zero line frequently even in the 22nd Century.

The prominence of interannual and decadal variations of PI (compared to the long-term changes) is not evident in the GFDL CM2.1 model only. Suppl. Figs. 1-3 show plumes of annual and five-year June-to-November SST (top panels) and PI (bottom panels) for the Scenario A1B integrations of the 22 IPCC-AR4 models used in this analysis. Notice that for each tropical basin and for each model, SST increases relatively monotonically. In contrast, PI changes in each basin show much more interannual and decadal variability relative to the long-term forced change in PI. In addition, for the chosen region in the Atlantic, the inter-model variations and the decadal swings are of sufficient magnitude that there is little consensus across the models of even the sign of the long-term PI change (Suppl. Fig. 1).

II. Proxy Index for PI:

We developed an index for changes in PI ($\widetilde{PI}$) by subtracting the tropical-mean SST change from the local SST change:

$$\widetilde{PI}(x,y,t) \equiv (\Delta SST'(x,y,t) - < \Delta SST'(t) >) \qquad (1)$$

where: $\Delta SST(x,y,t)$ is the SST anomaly, and $<\Delta SST(t)>$ is the 30°S-30°N spatially-averaged SST anomaly. A relationship is evident between $\widetilde{PI}$ and ΔPI for interannual to multi-decadal timescales in the climate models and reanalyses, suggesting that $\widetilde{PI}$ may be useful to estimate ΔPI changes on a broad range of timescales.

Here, we offer a table summarizing the relationships between $\widetilde{PI}$ and ΔPI for the two reanalysis products, and for the climate model projections for Scenario A1B from the IPCC-AR4. For the reanalysis products (ERA40 and NCEP) we compute the statistics based on the 1958-2002 linear least-squares trend of June-November SST and PI, for the IPCC-AR4 models we compute the statistics based on the model-projected June-November SST and PI changes between the 2081-2100 average and the 2001-2020 average. Statistics are computed over the region 30°S-30°N.

The statistics shown in the table are: the tropical-mean SST change ($<\Delta SST>$, with units of °C per 100years for the reanalyses, °C for IPCC-AR4 models) and tropical-mean PI change per unit tropical SST warming ($<\Delta PI>/<\Delta SST>$), the spatial correlation between *Bister and Emanuel [1998, 2002]* PI and $\widetilde{PI}$ changes ($r(\Delta PI, \widetilde{PI})$), and the slope ($m$) and intercept ($b$) of the linear regression between PI and $\widetilde{PI}$ (such that $\Delta PI(x,y) \cong m \cdot \widetilde{PI}(x,y) + b$). For references to the IPCC-AR4 models used, see Table 1 of *Vecchi and Soden [2007.b]*.

Model/Reanalysis Dataset	***<ΔSST>***	***<ΔPI>/ <ΔSST>***	***r(ΔPI, $\widetilde{PI}$)***	***m***	***b***
	(see text)	**ms^{-1}/°C**		**ms^{-1}/°C**	**ms^{-1}**
ERA40	**0.80**	**-0.63**	**0.87**	**8.55**	**-0.31**
NCEP	**0.72**	**-1.17**	**0.80**	**8.18**	**-0.89**
Ensemble-mean IPCC-AR4 Scenario-A1B	**1.71**	**0.33**	**0.84**	**8.22**	**0.56**
BCCR	1.74	0.74	0.89	8.11	0.74
CCCMA-T47	1.54	-0.10	0.86	7.92	-0.16
CCCMA-T63	1.78	0.17	0.85	8.39	0.30
CNRM	1.86	0.51	0.85	8.50	0.94
CSIRO-Mk3.0	1.35	0.50	0.89	7.34	0.68
CSIRO-Mk3.5	2.02	0.50	0.83	8.00	1.01
GFDL CM2.0	1.74	-0.34	0.88	6.54	-0.59
GFDL CM2.1	1.57	-0.83	0.87	6.64	-1.30
GISS-AOM	1.42	-1.17	0.60	8.40	-1.66
GISS-EH	1.30	-0.86	0.81	6.47	-1.12
GISS-ER	1.35	-0.86	0.78	7.01	-1.16
IAP FGOALS	1.39	0.85	0.92	9.49	1.17
INM CM3	1.39	0.96	0.80	7.06	1.33
INGV	1.48	-0.36	0.78	7.49	-0.53
IPSL CM4	2.10	0.84	0.85	8.81	1.76
MIROC Hi	2.75	1.34	0.91	10.94	3.79
MIROC Med	2.25	0.99	0.90	8.76	2.23
PI ECHAM5	2.33	-0.18	0.84	7.27	-0.42
MRI	1.58	1.09	0.86	10.67	1.65

NCAR CCSM3	1.43	0.91	0.86	9.68	1.30
NCAR PCM1	1.06	0.50	0.78	9.30	0.53
UKMO HadGem1	1.98	0.66	0.90	8.12	1.34

The relationships between SST changes and PI changes that justified the definition of $\widetilde{PI}$ (Eq. 1) suggests that localized SST changes will be more effective at impacting PI (per unit local warming) than relatively uniform temperature changes. This can be readily seen by considering four cases:

If the sign of ΔSST and <ΔSST> is the same, then:

i) Localized SST change. In this case $\left|\langle \Delta SST \rangle\right| << \left|\Delta SST\right|$, so $|\widetilde{PI}/\Delta SST| \sim 1$, and $\widetilde{PI}$ and ΔSST are of same sign.

ii) "Localized" remote SST change (*e.g.* El Niño impact on Atlantic). In this case $\left|\langle \Delta SST \rangle\right| >> \left|\Delta SST\right|$, so $|\widetilde{PI}/\Delta SST| > 1$, and $\widetilde{PI}$ and ΔSST are of opposite sign.

iii) Spatially uniform temperature change (*e.g.* response to GHG increase). In this case $\left|\langle \Delta SST \rangle\right| \sim \left|\Delta SST\right|$, so $|\widetilde{PI}/\Delta SST| < 1$, and the sign of $\widetilde{PI}$ and ΔSST can differ.

And a fourth case:

iv) If the sign of ΔSST and <ΔSST> differs (*e.g.,* localized aerosol cooling within global GHG warming), then $|\widetilde{PI}/\Delta SST| > 1$, and $\widetilde{PI}$ and ΔSST are of same sign.

III. Historical SST and $\widetilde{PI}$

We can exploit the proxy index for changes in PI ($\widetilde{PI}$, see Section II above), which we can use the observational SST reconstructions that are available from 1870s onwards to assess the implications of historical SST for long-term changes in PI. Since regional aspects of the long-term changes in SST differ across the reconstructions, we explore the $\widetilde{PI}$ changes exhibited by three different reconstructions (ERSST *[Smith and Reynolds 2003],* HadISST *[Rayner et al. 2003]* and LDEO-Kaplan *[Kaplan et al. 1998]*) to assess the impact of the inter-reconstruction differences on $\widetilde{PI}$.

Between the late-19th Century and the early-21st Century June-November SST has warmed throughout virtually the entire tropics (Suppl. Fig. 5.a-.c). The largest warming has been in the northern and near-equatorial Indian Ocean, and the southern tropical and near-equatorial Atlantic.

In contrast to the SST trends that are overwhelmingly positive, trends in June-November $\widetilde{PI}$ (Suppl. Fig. 5, lower panels) are mixed, highlighting the spatial heterogeneity of the warming and suggesting that the long-term changes in PI have included regions of both increase and decrease. For example, all three products have an increase in $\widetilde{PI}$ in the northern Indian Ocean, a decrease in the western tropical Pacific, and mixed changes in the tropical Atlantic (with regions of both increase and decrease). Thus, even in the presence of warming ocean temperatures over the last century, $\widetilde{PI}$ suggests that the thermodynamic environment in many regions has become less favourable for tropical cyclone intensification.

IV. Tropical-mean PI and SST:

By construction, the tropical-mean trend in $\widetilde{PI}$ is 0, whereas tropical-mean PI changes can be slightly nonzero (see Table above). However, both model projections and historical reanalyses indicate that the tropical-mean changes in PI are typically an order of magnitude smaller than the prominent regional changes. For example, the tropical-mean PI changes in the ERA40 and NCEP reanalysis products (-0.31 and -0.89 $ms^{-1}century^{-1}$, respectively) are considerably smaller than the typical regional values (compare to Suppl. Fig. 5). They also differ in sign from the ensemble-mean of IPCC-AR4 models, despite positive SST changes in all. In model projections for the 21st Century the sign of the tropical mean PI change also varies within models despite increasing tropical-mean SST (Supplementary Fig. 6), indicating that the tropical-mean changes in PI are not connected to the tropical-mean SST change in a simple manner. Thus, since there is no simple relationship between tropical-mean SST and PI changes, and since the tropical-mean PI changes in the reanalyses and model projections tend to be smaller than the regional changes, we propose $\widetilde{PI}$ as a useful first order approximation to changes in *Bister and Emanuel [1998, 2002]* PI.

References:

Bister, M. & K.A. Emanuel, Dissipative heating and hurricane intensity, *Meteorol. and Atmos. Phys.*, **65**(3-4), 233-240, doi: 10.1007/BF01030791, (1998).

Bister, M. & K.A. Emanuel, Low frequency variability of tropical cyclone potential intensity, 1, Interannual to interdecadal variability. *J. Geophys. Res.*, **107**, 4801, doi:10.1029/2001JD000776 (2002).

Kalnay, E., and co-authors, The NMC/NCAR 40-year reanalysis project, *Bull. Amer. Met. Soc.*, **77**, 437–471 (1996).

Kaplan, A., M. A. Cane, Y. Kushnir, A. C. Clement, M. B. Blumenthal & B. Rajagopalan, Analyses of global sea surface temperature 1856–1991. *J. Geophys. Res.*, **103**(C9), 18,567–18,589 (1998).

Rayner, N.A. and co-authors, Global analyses of sea surface temperature, sea ice, and night marine air temperature since the late nineteenth century, J. Geophys. Res., **108**, doi:10.1029/2002JD002670 (2003).

Smith, T.M. & R.W. Reynolds, Extended Reconstruction of Global Sea Surface Temperatures Based on COADS Data (1854-1997). *J. Climate*, **16**, 1495-1510 (2003).

Uppala, S. M., and co-authors, The ERA-40 reanalysis, *Q. J. R.Meteorol. Soc*., **131**, 2961–3012 (2005).

Vecchi, G.A. & B.J. Soden, Increased Tropical Atlantic Wind Shear in Model Projections of Global Warming. *Geophys. Res. Lett.,* **34**, L08702, doi:10.1029/2006GL028905 (2007.a).

Vecchi, G.A. and B.J. Soden, Global Warming and the Weakening of the Tropical Circulation, *J. Clim.*, **20**(17), 4316-4340 (2007.b).

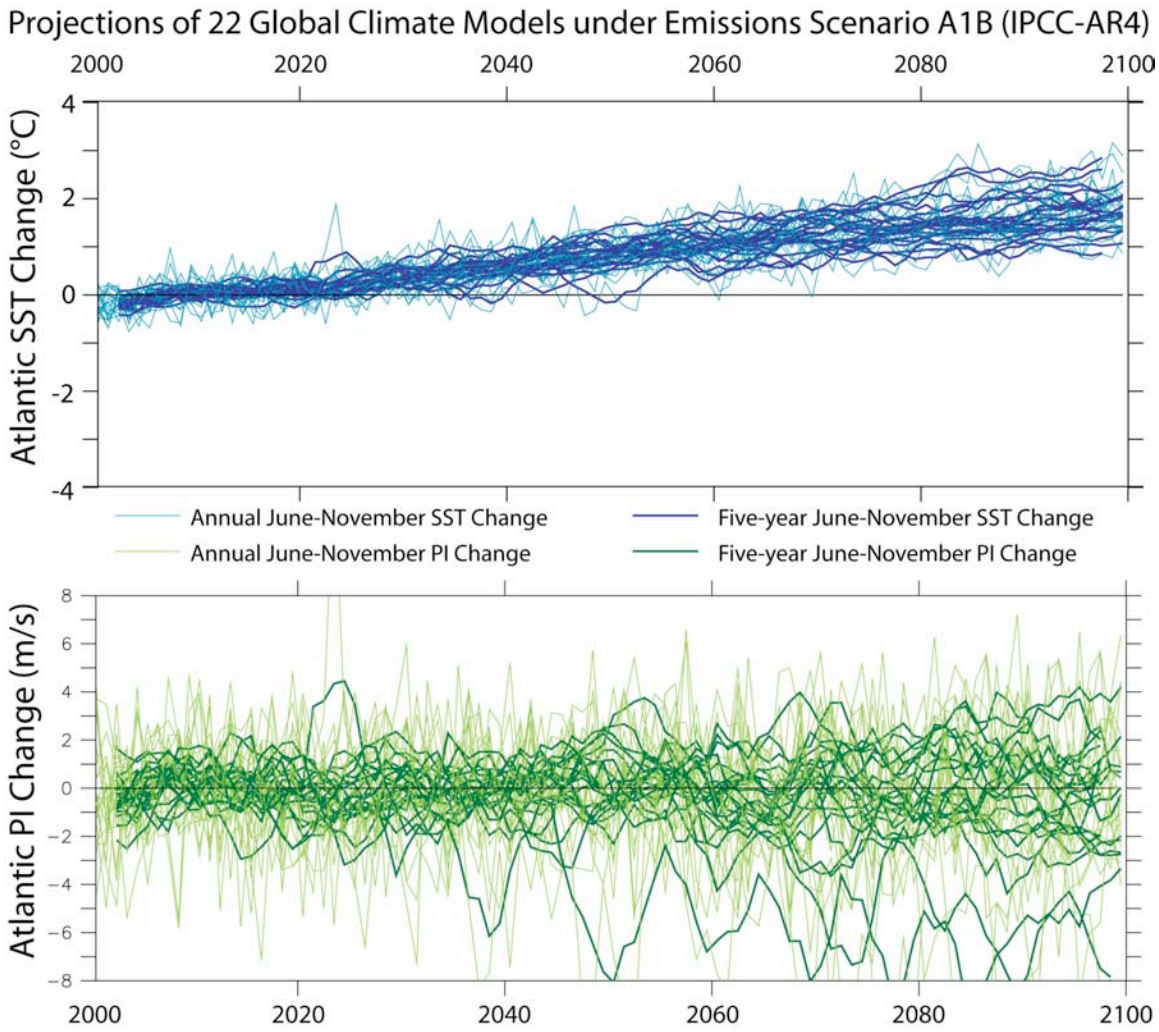

Supplementary Figure 1 Time series of North Atlantic (see Fig. 1.a) June-November change in SST (top panel, °C) and *Bister and Emanuel [1998]* PI (bottom panel, ms^{-1}) from each of the 22 IPCC-AR4 climate models under the A1B emissions scenario. Thin lines show the annual values, thick lines show the 5-year running mean. Changes computed from 2001-2020 average.

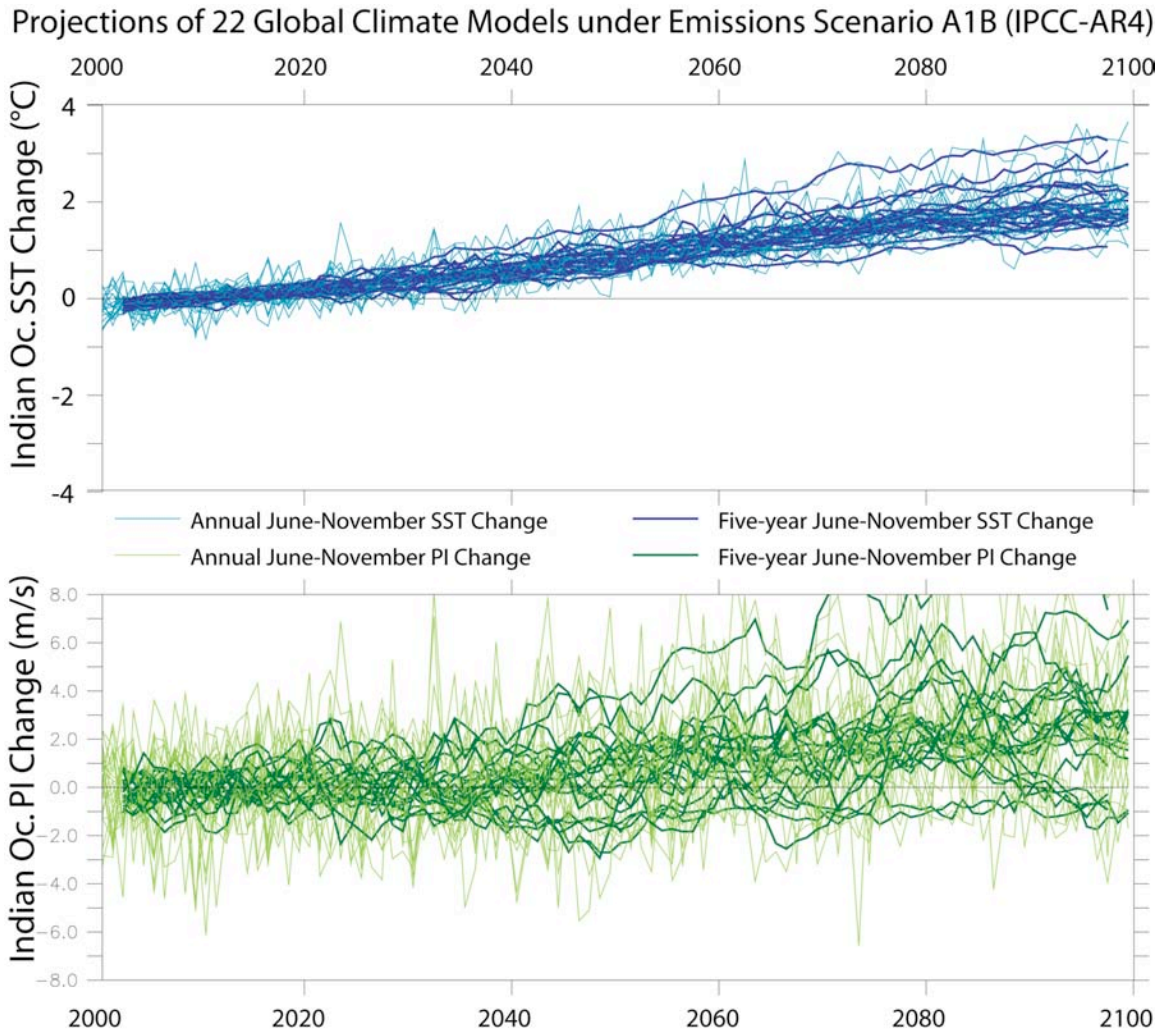

Supplementary Figure 2 Time series of West Pacific (see Fig. 1.a) June-November change in SST (top panel, °C) and *Bister and Emanuel [1998]* PI (bottom panel, ms^{-1}) from each of the 22 IPCC-AR4 climate models under the A1B emissions scenario. Thin lines show the annual values, thick lines show the 5-year running mean. Changes computed from 2001-2020 average.

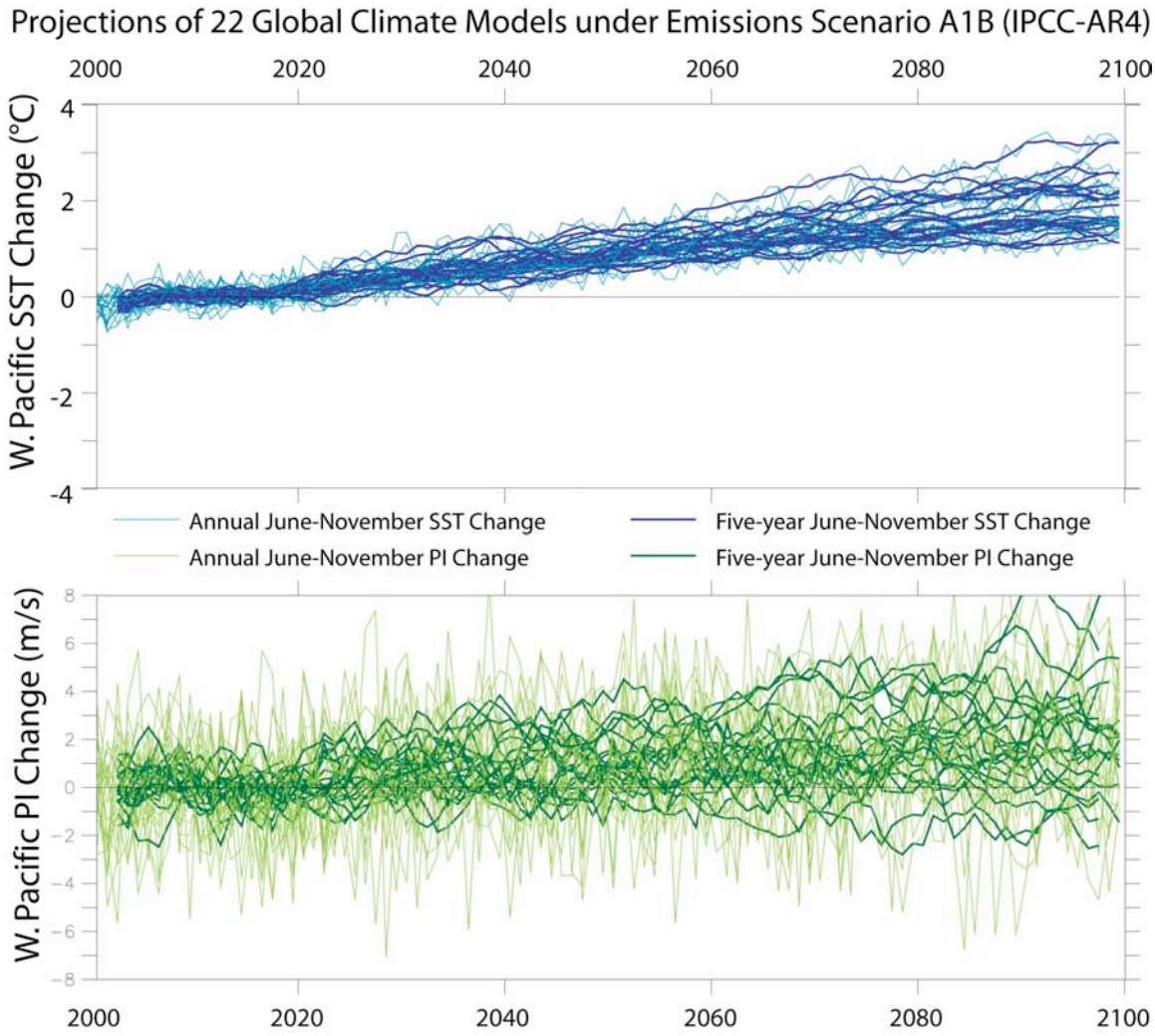

Supplementary Figure 3 Time series of Indian Ocean (see Fig. 1.a) June-November change in SST (top panel, °C) and *Bister and Emanuel [1998]* PI (bottom panel, ms^{-1}) from each of the 22 IPCC-AR4 climate models under the A1B emissions. Thin lines show the annual values, thick lines show the 5-year running mean. Changes computed from 2001-2020 average.

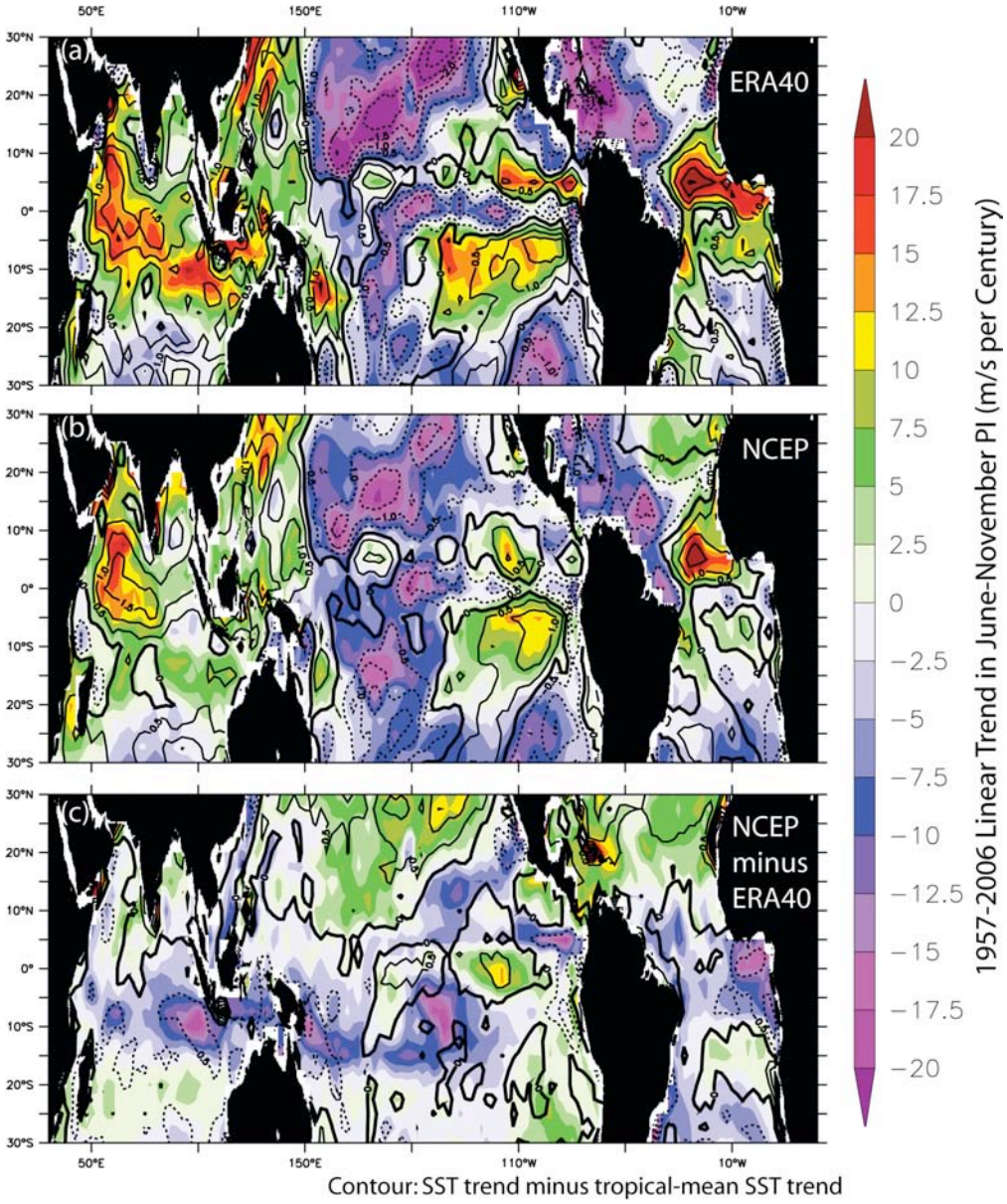

Supplementary Figure 4 Historical changes in SST and PI from two observational reanalyses. Linear trends in June-November computed from 1958-2002 for PI (shaded, $ms^{-1}century^{-1}$) and departure of local SST from tropical mean SST (contoured, $°C \cdot century^{-1}$, contour interval is 0.5°C per century) computed from ERA40 *[Uppala et al. 2005]* (top panel) and NCEP *[Kalnay et al. 1996]* (middle panel), the bottom panel shows the difference of NCEP minus ERA40. The spatial correlation coefficient between 1958-2002 SST changes and PI changes is 0.87 for ERA40 and 0.80 for NCEP.

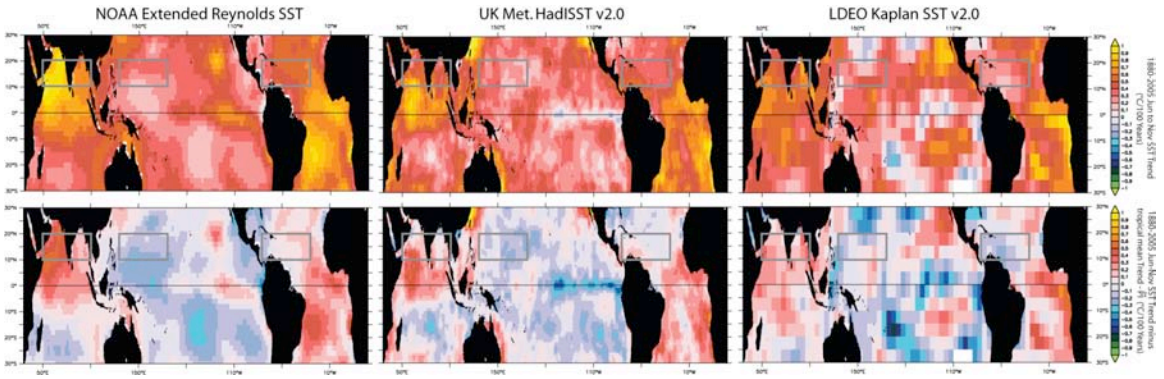

Supplementary Figure 5 Century-scale trends in SST and an estimate for PI ($\widetilde{PI}$). 1880-2006 linear trend in June-November SST (upper panels) and departure of local SST from tropical-mean SST (lower panels), computed using the SST reconstructions of *Smith and Reynolds [2003]* (left panels), *Rayner et al. [2003]* (middle panels), and *Kaplan et al. [1998]* (right panels). Units are °C·century^{-1}.

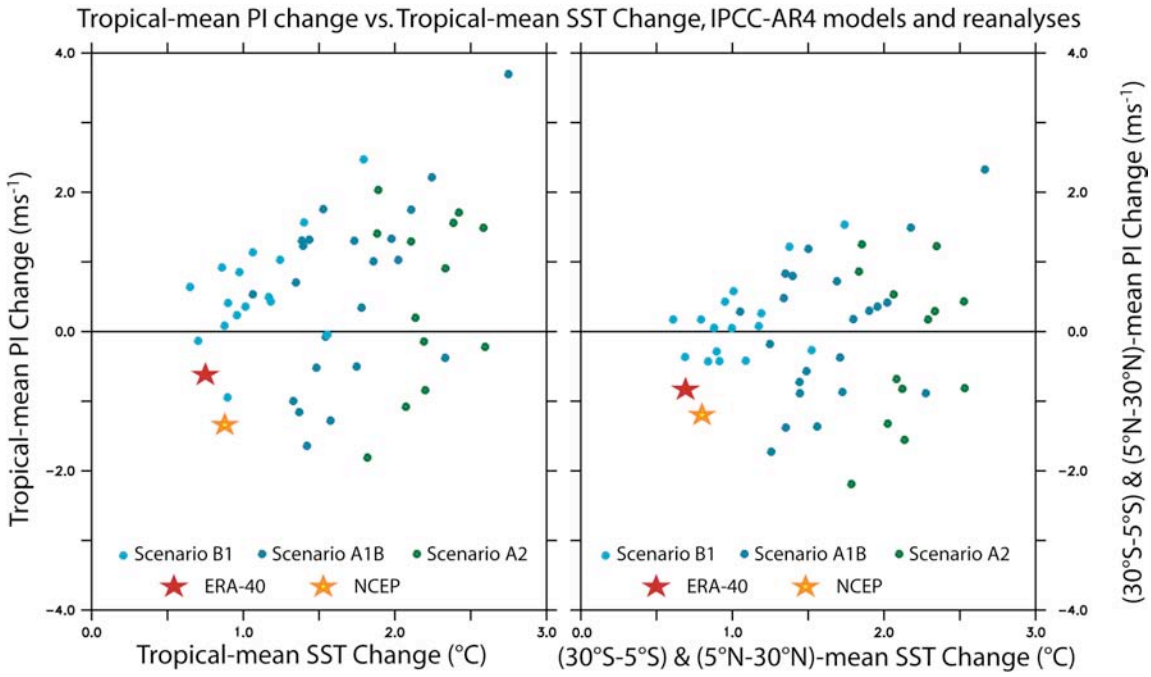

Supplementary Figure 5 Scatter plot of June-November tropical-mean SST vs. tropical-mean PI change for Scenarios A1B, A2 and B1 (blue dots) and for the NCEP (yellow star) and ERA40 (red star) reanalysis. Each dot represents the (2081-2100) minus (2001-2020) change from a single climate model from the IPCC-AR4 database, with different colors representing each of the three emissions scenarios. The stars are based on the 1958-2002 linear trends from each of the reanalysis products. Two scatter plots have been made, one for the entire tropics (left panel) and one highlighting the regions poleward of 5° latitude and equatorward of 30° latitude – since near the Equator the Coriolis parameter is not sufficiently large to allow for frequent tropical cyclone development.